Biodegradable xylitol-based elastomers: In vivo behavior and biocompatibility

Citation: Bruggeman, Joost P., Bettingera, Christopher J. and Langera, Robert. "Biodegradable xylitol-based elastomers: In vivo behavior and biocompatibility." Journal of Biomedical Materials Research 95A, 1 (October 2010): 92-104 © 2010 Wiley Periodicals.

As Published: http://dx.doi.org/10.1002/jbm.a.32733

Publisher: Wiley-Blackwell

Persistent URL: https://hdl.handle.net/1721.1/124682

Version: Author's final manuscript: final author's manuscript post peer review, without publisher's formatting or copy editing

Published in final edited form as:
J Biomed Mater Res A. 2010 October ; 95(1): 92–104. doi:10.1002/jbm.a.32733.

Biodegradable Xylitol-Based Elastomers: In Vivo Behavior and Biocompatibility

Joost P. Bruggeman[a,b], **Christopher J. Bettinger**[a,c], and **Robert Langer**[a,*]

[a] Department of Chemical Engineering, Massachusetts Institute of Technology, Cambridge, MA 02139, USA. [b] Department of Plastic and Reconstructive Surgery, Erasmus Medical Center, Erasmus University Rotterdam, 3015 GE, Rotterdam, The Netherlands. [c] Biomedical Engineering Center, Charles Stark Draper Laboratory, Cambridge, MA 02139, USA.

Abstract

Biodegradable elastomers based on polycondensation reactions of xylitol with sebacic acid, referred to as poly(xylitol sebacate) (PXS) elastomers have recently been developed. Herein, we describe the in vivo behavior of PXS elastomers. Four PXS elastomers were synthesized, characterized and compared to poly(L-lactic-*co*-glycolic acid) (PLGA). PXS elastomers displayed a high level of structural integrity and form stability during degradation. The in vivo half-life ranged from approximately 3 to 52 weeks. PXS elastomers exhibited increased biocompatibility compared to PLGA implants.

Keywords

Biomaterial; Elastomer; Biocompatibility; Degradation; Poly(xylitol sebacate); xylitol

1. Introduction

Synthetic biodegradable polyesters have become important materials in medicine and bio-engineering.1,2 Synthetic biodegradable polymers based on α-hydroxy acids such as glycolic and lactic acid exhibit a wide range of properties. For example, degradation rates for co-polymers based on these monomers can be tuned by altering their stoichiometry and molecular weights.3 Despite the widespread and immediate use of these polymers in surgery, tissue engineering and drug delivery,4 other monomers were introduced to realize more elastomeric materials, tailoring them for soft tissue applications.5,6 However, these thermoplastic polymers exhibit several drawbacks including bulk degradation and acidic byproducts.3,6,7 This also results in non-linear loss of mechanical properties versus mass loss, as well as loss of form stability and considerable construct swelling during degradation.3,6,8

We have recently developed a versatile platform of biodegradable elastomers, based on polycondensation reactions of xylitol with sebacic acid, referred to as PXS elastomers.9 PXS elastomers are composed of non-toxic monomers endogenous to the mammalian organism, but exhibit advantages of synthetic biomaterials. These advantages include rapid scalable synthesis as well as avoiding potential immune responses related to natural polymers such as collagen.10,11 In contrast to the previously reported poly(glycerol sebacate) (PGS) elastomer,7 we found that the degradation rate of PXS elastomers can be

* Corresponding author: rlanger@mit.edu Phone: (617) 253 3107 Fax: (617) 258 8827.

tuned by simple adjustments in chemical composition of PXS elastomers. We describe the synthesis and in vivo behavior of four PXS elastomers in this report: three PXS elastomer formulations were synthesized by altering the stoichiometric ratios of xylitol to sebacic acid. An additional polymer was produced through a co-polymerization strategy of two PXS pre-polymers with different stoichiometric ratios. We hypothesized that the bulk properties could be tuned through altering stoichiometry and polymer curing conditions. Furthermore, we speculated that the resulting set of PXS polymers would produce a wide range of in vivo half lives while maintaining in vivo biocompatibility. Throughout degradation, PXS elastomers displayed structural integrity and form stability. In vivo half-lives of these elastomers ranged from approximately 3 to 52 weeks. Based on evaluation of morphology and thermal properties of PXS implants, we propose an enzyme-driven degradation mechanism for PXS elastomers. In addition, PXS elastomers exhibited enhanced biocompatibility compared to PLGA.

2. Materials and Methods

2.1 Synthesis and characterization of PXS pre-polymers

All chemicals were purchased from Sigma-Aldrich (St. Louis, MO, USA) unless otherwise stated. Polymers with xylitol: sebacic acid ratios of 1:1, 2:3 and 1:2 were prepared, referred to as PXS 1:1, PXS 2:3 and PXS 1:2 respectively. Appropriate molar amounts of the polyol and reacting acid monomer were melted in a round bottom flask at 150 °C under a blanket of inert gas, and stirred for 2 h. Vacuum (~50 mTorr) was then applied yielding the pre-polymers PXS 1:1 (12 h), PXS 2: 3 (6 h) and PXS 1:2 (6 h) (Scheme 1A). The molecular weights of the pre-polymers were measured and compared to linear standards using gel permeation chromatography (GPC) using tetrahydrofuran on Styragel columns (series of HR-4, HR-3, HR-2, and HR-1, Waters, Milford, MA, USA). ^{1}H-NMR spectra were obtained of the PXS pre-polymers in C_2D_6O, on a Varian Unity-300 NMR spectrometer. The chemical composition of the pre-polymers was determined by calculating the signal integrals of xylitol, and compared to the signal integrals of sebacic acid. The signal intensities showed peaks of –OC$\underline{H}_2$(C$\underline{H}$(OR))$_3$C$\underline{H}_2$O– at 3.5 - 5.5 ppm from xylitol, and peaks of –COC$\underline{H}_2$C$\underline{H}_2$C$\underline{H}_2$– at 1.3, 1.6 and 2.3 ppm from sebacic acid.

2.2 Synthesis and characterization of PXS elastomers

All PXS pre-polymers were further cured by polycondensation, yielding the PXS 1:1, PXS 2:3 and PXS 1:2 elastomers. An additional elastomer was made from a 50/50 w/w mixture of PXS 1:1 and PXS 1:2 pre-polymers, yielding a PXS 1:1/1:2 co-polymer. The polycondensation was done at 120 °C and 140 mTorr for 4 days. Tensile tests were performed on dog-bone shaped polymer strips that were hydrated for at least 24 h in ddH_2O at 37 °C on an Instron 5542 (according to ASTM standard D412-98a). Differential scanning calorimetry (DSC) was performed as previously reported.9 Briefly, glass transition temperature (T_g) and other potential phase transitions were measured between -90 °C and 250 °C with a heating/cooling rate of 10 °C/min, using a Q1000 DSC equipped with Advantage Software v2.5 (TA Instruments, Newcastle, DE USA) and analyzed with Universal Analysis Software v4.3A (TA Instruments). The T_g measurements were performed on sol-free, dry elastomers, and therefore only resemble the thermal properties of the 'naked' degrading polymer network. The change of T_g over time (ΔT_g) was calculated by subtracting the T_g at the start of the experiment ($T_{g,\,t=0}$) from the T_g at time point t ($T_{g,\,t}$):

$$\Delta T_g = T_{g,t} - T_{g,t=0} \qquad \text{Equation 1}$$

The mass density was measured using a pycnometer (Humboldt, MFG. CO), and crosslink density (n) as well as the relative molecular mass between crosslinks (M_c) were calculated from the following equations for an ideal elastomer, where E_0 is the Young's modulus, R is the universal gas constant, T is the temperature and ρ is the mass density:

$$n=\frac{E_o}{3RT}=\frac{\rho}{M_c} \quad \text{Equation 2}$$

The water-in-air contact angle measurements were carried out as previously mentioned.12

2.3 In vivo implantation of PXS elastomers

Female Lewis rats (Charles River Laboratories, Wilmington, MA) weighing 200-250 g were housed in groups of 2 and had access to water and food *ad libitum*. Animals were cared for according to the approved protocols of the Committee on Animal Care of the Massachusetts Institute of Technology in conformity with the NIH guidelines for the care and use of laboratory animals (NIH publication #85–23, revised 1985). The animals were anaesthetized using continuous 2% isoflurane/O_2 inhalation. Two or three small midline incisions on the dorsum of the rat were performed and the implants were introduced in lateral subcutaneous pockets created by blunt dissection. The skin was closed using staples. Each rat carried either PXS 1:1, PXS 1:2 and PLGA, or PXS 2:3, PXS 1:1/1:2 and PLGA implants. The animals were inspected daily until post-operative day 10 for early wound healing problems. Throughout the study, all rats stayed in good general health as assessed by their weight gain.

2.3 In vivo degradation and biocompatibility of PXS elastomers

For the degradation study, PXS elastomeric discs (diameter 10×1.6 mm) ($n=4$) were implanted subcutaneously in rats. As a control, PLGA (65/35 high M_w, inherent viscosity 0.60 – 0.80 dL/g, Lakeshore Biomedical, Birmingham, AL, USA) pellets were melt-pressed (0.5 g, 172 °C, 5000 MPa) into a mold (d = 10 mm, h = 1.5 mm) using a Carver Hydraulic Unit Model #3912-ASTM (Carver, Inc. Wabash, IN). Before implantation, polymer discs were weighed (M_0) and their thickness (H_0) was measured between two glass cover slides using calipers. To investigate in vivo degradation, implants were harvested at pre-determined time points and collected in sterile saline. Directly upon surgical removal, the explants were dabbed dry, weighed (M_{wet}), and their thickness (H_t) was measured again. The explants were then dried at 90 °C for 3 days and weighed (W_{dry}) again. Water content (hydration) by mass and implant dimensions at time point t were calculated as follows:

$$\frac{M_{wet}-M_{dry}}{M_{dry}}\times 100\% \quad \text{Equation 3}$$

for water content, and

$$\frac{|H_t-H_0|}{H_0}\times 100\% \quad \text{Equation 4}$$

for implant size.

The in vivo mass loss over time was calculated using equation 5:

$$\frac{M_0 - M_{dry}}{M_0} \times 100\%$$ Equation 5

Compression tests were performed on the wet explants with a 50N load cell at a compression rate of 5 mm/min using an Instron 5542, according to ASTM standard D575-91. All samples were compressed to 50 N and the compression modulus was calculated from the initial slope (0 - 10 %) of the stress-strain curve. The compression modulus was determined before implantation, and the ratio of the initial modulus was calculated to the modulus at the pre-determined time point (E_t) as follows:

$$\frac{E_t}{E_0} \times 100\%$$ Equation 6

Explants dedicated for scanning electron microscopy (SEM) were sputter-coated with platinum/palladium (≈250A), mounted on aluminum stubs with carbon tape, and examined on a JEOL JSM-5910. Explants dedicated to determine sol content were weighed (M_{dry}), placed in 100% ethanol for 3 days on a orbital shaker, dried at 90 °C for 1 day and weighed ($M_{solfree}$) again. The sol content of the explants was calculated, using the following equation:

$$\frac{M_{dry} - M_{solfree}}{M_{solfree}} \times 100\%$$ Equation 7

For biocompatibility analysis, explants and surrounding tissues were harvested, and fixed in Accustain for 24 h, dehydrated in graded ethanol (70 - 100%), embedded in paraffin, sectioned using a microtome (4 μm). Sequential sections (8-15 μm) were stained with hematoxilyn and eosin (H&E). The H&E stains were used to analyze for the presence of fibroblasts and neutrophils in the tissues surrounding the material, and for the presence of multinucleated giant cells, ingrowth of cells into the material as well as phagocytosis of the material. Tissue macrophages were identified by staining sections with primary rabbit anti-rat CD6813 (1:200, Abcam, England UK), followed by goat anti-mouse secondary antibody (Vector Burlingame, CA USA). Samples were incubated with streptavidin horseradish peroxidase (1:100, Dako, Denmark) and developed with DAB substrate chromogen (Dako). Histology images were recorded with a Zeiss CCD Camera equipped with Axiovision software (Zeiss, Germany).

2.4 Statistical analysis

At least four fibrous capsule thickness measurements were made across at least ten randomly selected images per time point per sample, and the number of CD68+ macrophages was similarly based on at least ten randomly selected images per time point per sample. Non-parametric two-way ANOVA tests were performed where appropriate (GraphPad Prism 4.02, GraphPad Software, San Diego, CA USA). Dunn's multiple comparison post-tests were used to determine significance between specific treatments. All graphical data is reported as mean ± S.D. Significance levels were set at * $p < 0.05$.

3. Results

3.1 Pre-polymer synthesis and characterization

PXS pre-polymers (Scheme 1A) and their chemical compositions were confirmed by ^{1}H-NMR spectra. Molecular weight distributions determined by GPC are summarized in Table 1 as well. PXS pre-polymers have accessible melting temperatures (T_ms), allowing for processing and mixing pre-polymers. The temperatures used for processing are listed in Table 1. A blend of PXS 1:1 and PXS 1:2 at 50/50 w/w was prepared additionally and, similar to the PXS 1:1, PXS 2:3 and PXS 1:2 pre-polymers, further cured into elastomeric networks (Scheme 1B).

3.2 Characterization of PXS elastomers

PXS 1:1, PXS 2:3 and PXS 1:2 elastomers as well as the PXS 1:1/1:2 co-polymer revealed stress strain curves as shown in Supplementary Figure 1. Tensile Young's moduli ranged from 0.82 ± 0.15 to 5.33 ± 0.40 MPa as previously reported for PXS 1:1 and PXS 1:2 elastomers.9 The PXS 1:1/1:2 and PXS 2:3 elastomer revealed Young's moduli of 2.32 ± 0.27 and 3.42 ± 0.13 MPa respectively, and fall within the limits defined by the PXS 1:1 and 1:2 elastomers. The mechanical properties of PXS elastomers are summarized in Table 2. T_gs ranged from a lower limit of PXS 1:1 (7.3 °C) to an upper limit value of PXS 1:2 (22.9 °C) and in between these limits were the values of the PXS 1:1/1:2 (18.7 °C) and PXS 2:3 (20.2 °C) elastomers. The molecular weight between crosslinks revealed a similar trend: PXS 1:2 had the lowest molecular weight between crosslinks (M_c, 1585.1 ± 43.7 mol/m^3), PXS 1:1 the highest (10517.4 ± 102.1 mol/m^3) and in between were the values for PXS 1:1/1:2 (3685.7 ± 90.5 mol/m^3) and PXS 2:3 (2521.6 ± 100.5 mol/m^3). The contact angle measurements and in vitro hydration (determined by mass differential), followed the same trend: PXS 1:1 exhibited the lowest contact angle and highest hydration by mass (26.5 ± 3.6° and 12.6 ± 0.4%), PXS 1:2 the highest contact angle with the lowest hydration (52.7 ± 5.7° and 4.1 ± 0.3%) and PXS 1:1/1:2 and PXS 2:3 (31.6 ± 4.3°, 8.3 ± 1.6% and 43.8 ± 2.2°, 3.7 ± 0.9% respectively) in between the values of PXS 1:1 and PXS 1:2. The physical properties of PXS elastomers are summarized in Table 2.

3.3 In vivo degradation of PXS elastomers

Similarly, the trends of the in vivo mass loss, hydration by mass, sol content, loss of mechanical properties, and implant thickness over time were also confined by limits set by the PXS 1:1 and PXS 1:2 elastomers, with the values of PXS 1:1/1:2 and PXS 2:3 elastomers within these limits. The in vivo half life of PXS 1:1 implants was approximately 3 to 4 weeks, and revealed a roughly linear decrease in mass over time (Figure 1A). PXS 1:2 implants degraded much slower, with 76.7 ± 3.7% of its original dry weight remaining after 28 weeks in vivo. The in vivo mass loss of PXS 1:1 and 1:2 was published recently.9 PXS 1:1/1:2 implants appeared to have a mass loss profile that was a combination of the separate PXS 1:1 and PXS 1:2 elastomers: it had an in vivo half life of approximately 15 weeks and had almost completely degraded at 27 weeks (Figure 1A). PXS 2:3 implants had a projected half life of approximately 30 weeks, and similar to the PXS 1:2 elastomers, showed an initial lag time where no mass loss was observed, after which a linear decrease in mass was observed (Figure 1A).

PXS implant thickness during degradation gradually diminished over time, meaning that these polymers do not extensively swell in vivo (Figure 1B). Hydration of PXS elastomers was relatively mild and never exceeded 40% of the dry mass (Figure 1C). PXS 1:1 implants showed the highest hydration during degradation. The PXS 1:1/1:2 co-polymer, as well as the PXS 2:3 and PXS 1:2 elastomers demonstrated similar hydration profiles (Figure 1C).

Thermoset polymer networks contain a fraction of loose, entangled macromers that are not covalently attached to the polymer network, referred to as the sol fraction. Upon degradation of polyesters, scission of esters bonds occurs which can potentially increase a network's sol fraction.14 This behavior was observed for all PXS elastomers in vivo: sol fractions were observed to increase over time, being at their highest values near complete degradation, but never exceeding 30% of the dry mass (Figure 1D).

The compression moduli of PXS elastomers decreased with time as expected, with the exception of PXS 1:2 (Figure 1E). At 23.3 ± 3.7% mass loss of PXS 1:2 implants, no deterioration in compression modulus was observed. When PXS 1:1 elastomers had degraded 24.7 ± 11.0% however, a decrease of 35.2 ± 4.7% of their original compression modulus was observed. The relationship between mass loss and mechanical properties for all four PXS elastomers (Supplementary Figure 2) demonstrated a different trend for the PXS 1:2 elastomers in comparison to the other elastomers. Unlike PXS 1:2, the mechanical properties of PXS 1:1, PXS 1:1/1:2 and PXS 2:3 decreased in a roughly linear manner as the material degraded.

ΔT_gs of PXS elastomers over time were initially negative, and then increased with time as degradation occurred, displayed by PXS 1:1/1:2, PXS 2:3 and PXS 1:2 (Figure 1F). An initial negative ΔT_g however, was not observed for PXS 1:1 elastomers.

3.4 Morphological assessment of PXS and PLGA implants

PXS elastomers appeared smooth-surfaced and optically clear at early time points upon visual inspection. Surfaces appeared progressively rough, and implants became more opaque as degradation progressed. Observation of gross morphology revealed that PXS elastomers maintained a high level of structural integrity and form stability compared to PLGA implants during degradation (Figure 2A-J). The in vivo mass loss of PLGA implants used in this study, as well as deterioration of mechanical properties and construct swelling by mass over time, are shown in Supplementary Figure 3.

Surface analysis through SEM revealed a degradation front that progressed inward from the surface (PXS 1:1 and PXS 1:2 elastomers are shown) (Figure 3A-F). After 1 week, surfaces of PXS 1:1 elastomers showed excavates whilst the interior of the implant seemed intact (Figure 3A). When PXS 1:1 implants had lost more than 76.7 ± 3.7% of their initial mass, a more porous surface covered with excavates was observed (Figure 3B). After 5 weeks in vivo, PXS 1:2 implants had demonstrated no perceptible mass loss or changes in the morphology of the surface or bulk (Figure 3C). When PXS 1:2 implants degraded however, a rough surface was observed, but the pores appeared smaller as compared to the degrading PXS 1:1 surfaces (Figure 3D). The general morphology of degrading PXS implants contrasted that of degrading PLGA implants significantly. PLGA implants showed signs of bulk degradation and the absence of surface erosion (Figure 3E, F).

3.5 In vivo biocompatibility of PXS 1:1 and 1:2

An initial biocompatibility study of PXS 1:1 and PXS 1:2 elastomers was reported previously, and demonstrated in vivo biocompatibility compared to PLGA implants.9 Here, we studied the biocompatibility in more detail. Following implantation, none of the animals showed post-operative abnormalities in their wound healing process. At all time points during the in vivo experiment, PXS implants were encased by a very thin, translucent fibrous capsule, which appeared thicker macroscopically for PLGA implants. On autopsy, occasional vascularization of the capsule was observed for PXS implants, but this seemed more prominent for PLGA implants. The surrounding tissues of both PXS and PLGA implants appeared normal clinically. Microscopic evaluation of the histological specimen

revealed a thin fibrous capsule surrounding PXS 1:1 elastomers after 1 week in vivo (Figure 4A). When examined in more detail (insert of Figure 4A shown in Figure 4B), this capsule seemed to consist mainly of lymphocytes, macrophages and fibroblasts. The degradation products did not seem to influence fibrous capsule thickness at time points where significant mass loss for PXS 1:1 elastomers was observed (5 weeks, Figure 4C). However, the fibrous capsule did show signs of chronic inflammation with fewer lymphocytes, macrophages and giant cells at the polymer surface, as shown at 20x magnification (Figure 4D). This thin fibrous capsule was predominantly composed of fibroblasts and vascularization of this capsule was not obvious. A very similar tissue response was observed for fibrous capsules surrounding the PXS 1:2 elastomers, despite their slower degradation rate (Figure 5A). Lymphocytes, macrophages and fibroblasts were visible in this capsule, demonstrating the similar wound healing response as PXS 1:1 implants. Also, PXS 1:2 did not induce noticeable infiltration in the surrounding tissues (Figure 5B). After 28 weeks of implantation time, PXS 1:2 elastomers were still encased by a thin fibrous capsule (Figure 5C). At the corners of the implants, where most friction with surrounding tissues is expected, fibrous capsules of less than 20 cell layers thick were observed (Figure 5D). The fibrous capsules were also mostly composed of fibroblasts with few scattered macrophages and giant cells at the polymer/ tissue interface. PLGA implants however, showed fibrous capsules that were evidently vascularized after 1 week in vivo (Figure 6). In addition, tissues not in direct contact with the implants demonstrated infiltration with mononuclear cells (Figure 6A, B). This response was not observed for PXS elastomers. Upon degradation of PLGA implants at 12 weeks in vivo, fibrous capsules appeared thicker (Figure 6C) and contained higher numbers of macrophages and giant cells compared to PXS elastomers. In addition, evident phagocytosis of polymer was observed during polymer degradation, which was not the case for PXS elastomers (Figure 6D).

The biocompatibility of PXS implants was quantitatively higher than PLGA implants based on fibrous capsule thickness surrounding the implants as well as less infiltration of activated macrophages. Figure 7 demonstrates differences in fibrous capsule thicknesses: at week 1, PXS 1:1 and 1:2 were surrounded by significantly thinner capsules than PLGA (* $p < 0.05$), as measured by non-parametric two-way ANOVA. No significant difference in fibrous capsule thickness at week 2 was observed between the PLGA and PXS implants ($p > 0.05$). Also, there was no difference in capsule thickness between the PXS elastomers at week 5 ($p > 0.05$). At week 12, as well as week 27 for PXS 1:2, fibrous capsules surrounding the PXS elastomers were significantly thinner than capsules around PLGA implants (** $p < 0.05$).

When histological specimen were stained for the presence of CD68 (a marker for activated macrophages), a marked difference was observed between PXS elastomers and PLGA polymers, both qualitatively (Figure 8A-I) and quantitatively (Figure 9). Significantly less macrophages were recruited by PXS 1:1 and PXS 1:2 than PLGA at week 1 (* $p < 0.05$ for PXS 1:1, ** $p < 0.001$ for PXS 1:2), but not at week 2 between PXS 1:1 and PLGA implants ($p > 0.05$), determined by two-way ANOVA. Interestingly, the fraction of CD68+ cells surrounding PXS 1:2 was lower than PXS 1:1 at week 1 ($p < 0.05$) and PLGA implants at week 2 (§ $p < 0.05$). When degradation advanced however, PXS 1:1 (at week 5) revealed significant less CD68+ cells compared to degrading PLGA implants at week 12 ($p < 0.05$). The number of CD68+ cells surrounding the PXS 1:2 was also significantly less than the number of activated macrophages surrounding PLGA implants at week 12 (*** $p < 0.001$) (Figure 9).

4. Discussion

Tuning the in vivo behavior of biodegradable polymers is important to meet application-specific demands.[9,15] This proved to be straightforward for PXS elastomers and was

demonstrated by adjusting monomer feed ratios as well as by co-polymerization of pre-polymers with different stoichiometries. Taking step-growth polymer kinetics into account, and using the hydroxyl groups as the dominant functionality by 1, the PXS 1:2 stoichiometry shown here represented an upper limit of accessible crosslinking densities for PXS elastomers. As the ratio of aliphatic monomers (sebacic acid) in the polymerization reaction was increased to alter crosslink density, changes in glass transition, tensile Young's – and compression modulus, as well as contact angles, and therefore changes in degradation rates were observed.16 Similar to reported degradation rates for FDA approved medical devices composed of thermoplastic polymers such as PLGA3 and poly($^{50}/_{50}$ ($^{85}/_{15}$ D/L)-lactic-*co*-ε-caprolactone),8 subcutaneous degradation rates of PXS elastomers could be tuned from 7 weeks (PXS 1:1), up to a projected in vivo life time of approximately 2 years (PXS 1:2) (Figure 1A). Bulk degrading materials such as PLGA can reveal a non-linear deterioration in mechanical properties after an initial lag time, before significant mass loss has been achieved.3,8,17 PXS elastomers never exhibited this in vivo behavior. Mass loss and loss of mechanical properties were roughly linear, whereas PXS 1:2 implants retained their mechanical properties throughout the initial 23.3 ± 3.7% mass loss (Supplementary Figure 2). Furthermore, the presented degradation rates were accessible for PXS elastomers without consequences in construct swelling (Figure 1C) or form stability during degradation (Figure 2 and 3). This is an important advantage for small-feature medical devices such as flexible drug eluting chips and biosensors,18 peripheral nerve conduits19 and small vascular grafts. 20 In addition, through co-polymerization of pre-polymers, we have demonstrated PXS elastomers with relatively similar mechanical properties (PXS 1:1/1:2 and PXS 2:3) and different degradation rates (Table 2, Figure 1, Supplementary Figure 1). To this date, tuning degradation rate as well as decoupling degradation rate with mechanical properties as demonstrated here has not been shown for comparable thermoset elastomers, *e.g.* PGS. Therefore, PXS elastomers offer a platform of elastomers of which the in vivo properties can be tuned to meet a broad variety in application-specific demands.

Although the T_g of some PXS elastomers rose close to 37 °C during degradation, PXS implants were observed to remain in a rubbery state at room temperature, most likely due to T_g suppression from the presence of plasticizers including water and molecules that compose the sol fraction.15 The value of ΔT_g of PXS elastomers was observed to be initially negative, but eventually trended positive during in vivo degradation. This implies that there are multiple events which lead to counteracting trends in ΔT_g. Decreases in ΔT_g ($\Delta T_g < 0$) are thought to arise from the following modifications to the polymer network: (1) reduction in crosslink density through cleavage of crosslinked chains; (2) increase in free volume through dissociation and subsequent removal of polymer sol. Increases in T_g ($\Delta T_g > 0$) could arise to other types of network modifications upon degradation: (1) reduction of freely rotating polymer chains due to the cleavage of exposed polymer segments;21 (2) increased hydrogen bonding due to increased formation of hydroxyl and carboxylic acid groups upon ester cleavage.22,23 Thus, the observed kinetics of T_gs of most PXS elastomers suggest that degradation mechanisms initially reduce the T_g, but that degradation mechanisms increasing T_g eventually dominated. The PXS 1:1 elastomer however never demonstrated this initial decrease in T_g.

The overall trend in T_g can be explained by considering two types of degradation events: hydrolysis of ester bonds and enzymatic scission via esterase activity, acting across two different phases of the polymer construct. Some appreciable volume fraction of the polymer is able to be accessed by enzymes which can then work to degrade the polymer at localized surfaces. Conversely, the volume fraction that is not able to be accessed by diffusion of enzymatic species throughout the network is degraded primarily through hydrolysis. Enzymatic activity on polyesters is hypothesized to work primarily to increase the T_g by reducing the amount of mobile polymer chains attached to the network.21,24,25 Hydrolysis

is thought to work primarily to decrease the T_g by widespread reduction of crosslink density as random scission occurs throughout the network. Both enzymatic activity and hydrolysis can lead to increasing T_g through the possibility of increased hydrogen bonding. As previously reported,26 PXS 1:1 elastomers revealed a negligible in vitro mass loss after 105 d in PBS at 37 °C. This observed discrepancy with the in vivo mass loss profile for PXS 1:1 elastomers suggests that the degradation mechanisms may be dominated by an enzyme-driven degradation of PXS elastomers.17 The exact mechanism of degradation will need to be explored further by comparing the effects on T_g of controlled in vitro degradation conditions as well as additional polymers of varied chemical composition with the observed in vivo trends.21

Subcutaneously placed PXS elastomers revealed improved biocompatibility when compared to PLGA implants, as PXS implants recruited less activated macrophages and were encased by thinner fibrous capsules (Figure 5 – 9). Histology however revealed tissue reactions typical of a foreign body response to implants. In general, it is thought that materials with higher moduli result in harsher tissue reactions.12 This is also demonstrated by the differences in fibrous capsule thickness between PLGA and PXS implants. Interestingly, the in vivo biocompatibility profiles of PXS 1:1 and 1:2 elastomers were not completely comparable: PXS 1:2 elastomers revealed significant lower CD68+ cell numbers surrounding the implants, compared to PXS 1:1 at all time points (Figure 9). This indicates that the more slowly degrading PXS elastomers are better tolerated by the host tissue, despite the higher Young's modulus of PXS 1:2 elastomers compared to PXS 1:1. The different numbers of activated macrophages found in this study may be due to a difference in quantity (PXS 1:1 vs PXS 1:2) as well as chemical composition (PLGA vs PXS) of the degradation products.

5. Conclusions

Biodegradable PXS elastomers revealed precise control of material properties by adjusting the stoichiometric ratios as well as through co-polymerization of different stoichiometries. A wide range of in vivo degradation rates and mechanical properties were achieved. We hypothesize that in vivo degradation of PXS elastomers occurred predominantly through an enzyme-driven degradation mechanism. PXS elastomers retained structural integrity and form stability during degradation. In addition, PXS elastomers revealed biocompatibility, demonstrated by thinner fibrous capsules as well as lower numbers of activated macrophages surrounding the implants, compared to PLGA. These results suggest that the reduced fibrous wall thickness and macrophage recruitment in vivo are enabling properties of PXS elastomers, which makes them potentially suitable for biodegradable medical devices that require structural integrity and form stability for use in short, as well as long-term implantation applications.

Supplementary Material

Refer to Web version on PubMed Central for supplementary material.

Acknowledgments

J.P.B. acknowledges financial support from the J.F.S. Esser Stichting and the Stichting Prof. Michaël-Van Vloten Fonds. CJB was funded by a Charles Stark Draper Laboratory Fellowship. This work was funded by NIH grant HL060435 and through a gift from Richard and Gail Siegal.

7 References

1. Langer R, Vacanti JP. Tissue engineering. Science. 1993; 260(5110):920–6. [PubMed: 8493529]

2. Scott M. 32,000 years of sutures. NATNEWS. 1983; 20(5):15–17. [PubMed: 6346101]
3. Middleton JC, Tipton AJ. Synthetic biodegradable polymers as orthopedic devices. Biomaterials. 2000; 21:2335–2346. [PubMed: 11055281]
4. Langer R. Drug delivery and targeting. Nature. 1998; 392(6679 Suppl):5–10. [PubMed: 9579855]
5. Den Dunnen WF, Van der Lei B, Schakenraad JM, Blaauw EH, Stokroos I, Pennings AJ, Robinson PH. Long-term evaluation of nerve regeneration in a biodegradable nerve guide. Microsurgery. 1993; 14(8):508–515. [PubMed: 8271930]
6. Pêgo, AP. Biodegradable Polymers Based On Trimethylene Carbonate For Tissue Engineering Applications. University of Twente; Enschede: 2002.
7. Wang Y, Kim YM, Langer R. In vivo degradation characteristics of poly(glycerol sebacate). J Biomed Mater Res A. 2003; 66(1):192–7. [PubMed: 12833446]
8. Den Dunnen WFA, Meek MF, Grijpma DW, Robinson PH, Schakernraad JM. In Vivo and in vitro degradation of poly[50/50(85/15 L/D)LA/ε-CL], and the implications for the use in nerve reconstruction. J Biomed Mater Res A. 2000; 51:575–585.
9. Bruggeman JP, Bettinger CJ, Nijst CLE, Kohane DS, Langer R. Biodegradable Xylitol-Based Polymers. Adv Mater. 2008; 20(10):1922–1927.
10. Badylak SF. The extracellular matrix as a biologic scaffold material. Biomaterials. 2007; 28(25): 3587–3593. [PubMed: 17524477]
11. Ellingsworth LR, DeLustro F, Brennan JE, Sawamura S, McPherson J. The human immune response to reconstituted bovine collagen. J Immunol. 1986; 136(3):877–882. [PubMed: 2416836]
12. Wang Y, Ameer GA, Sheppard BJ, Langer R. A tough biodegradable elastomer. Nat Biotechnol. 2002; 20(6):602–606. [PubMed: 12042865]
13. Greaves DR, Gordon S. Macrophage-specific gene expression: current paradigms and future challenges. Int J Hematol. 2002; 76(1):6–15. [PubMed: 12138897]
14. Amsden B. Curable, biodegradable elastomers: emerging biomaterials for drug delivery and tissue engineering. Soft Matter. 2007; 3:1335–1348.
15. Bettinger CJ, Bruggeman JP, Borenstein JT, Langer R. Amino alcohol-based degradable poly(ester amide) elastomers. Biomaterials. 2008; 29(15):2315–2325. [PubMed: 18295329]
16. Pitt CG, Hendren RW, Schindler A, Woodward SC. The enzymatic surface erosion of aliphatic polyesters. J Control Release. 1984; 1:3–14.
17. Amsden BG, Tse MY, Turner ND, Knight DK, Pang SC. In vivo degradation behavior of photo-cross-linked star-poly(epsilon-caprolactone-co-D,L-lactide) elastomers. Biomacromolecules. 2006; 7(1):365–372. [PubMed: 16398537]
18. LaVan DA, McGuire T, Langer R. Small-scale systems for in vivo drug delivery. Nat Biotechnol. 2003; 21:1184–1191. [PubMed: 14520404]
19. Meek MF, Coert JH. US Food and Drug Administration/Conformit Europe-Approved Absorbable Nerve Conduits for Clinical Repair of Peripheral and Cranial Nerves. Ann Plast Surg. 2008; 60:110–116. [PubMed: 18281807]
20. Yang J, Webb AR, Pickerill SJ, Hageman G, Ameer GA. Synthesis and evaluation of poly(diol citrate) biodegradable elastomers. Biomaterials. 2006; 27(9):1889–98. [PubMed: 16290904]
21. Bettinger CJ, Bruggeman JP, Borenstein JT, Langer R. In vitro and in vivo degradation of poly(1,3-diamino-2-hydroxypropane-co-polyol sebacate) elastomers. J Biomed Mater Res A. Dec 23.2008 [Epub ahead of print].
22. Forrest JA, Dalnoki-Veress K, Stevens JR, Dutcher JR. Effect of free surfaces on the glass transition temperature of thin polymer films. Phys Rev Lett. 1996; 77(10):2002–2005. [PubMed: 10061832]
23. Keddie JL, Jones RAL, Cory RA. Interface and surface effects on the glass-transition temperature in thin polymer films. Faraday Discuss. 1994; 98:219–230.
24. Wang Z, Wang S, Guidoin R, Marois Y, Zhang Z. In vitro homogeneous and heterogeneous degradation of poly(epsilon-caprolactone/polyethylene glycol/L-lactide): the absence of autocatalysis and the role of enzymes. J Biomed Mater Res A. 2006; 79:6–15. [PubMed: 16741981]
25. Williams DF. Mini-review: enzyme-polymer interactions. J Bioeng. 1977; 1:279–294.

26. Bruggeman JP, De Bruin BJ, Bettinger CJ, Langer R. Synthesis and Characterization of Biodegradable Poly(polyol sebacate) Polymers. Biomaterials. 2008; 29(36):4726–4735. [PubMed: 18824260]

A

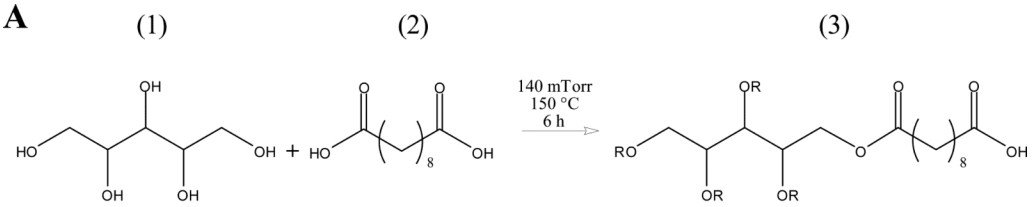

Stoichiometric ratios of (1) and (2)

1	:	1	⟶	PXS 1:1
2	:	3	⟶	PXS 2:3
1	:	2	⟶	PXS 1:2

B

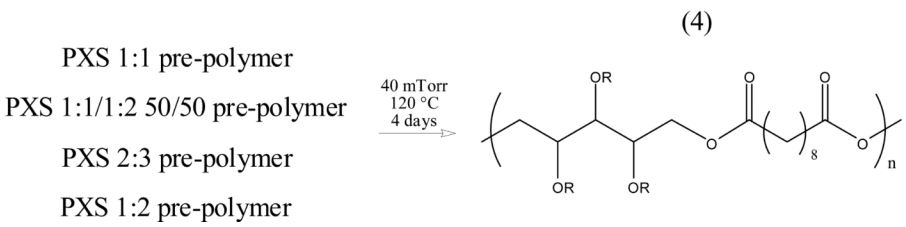

Scheme 1.

General synthetic scheme for PXS elastomers. **(A)** Xylitol **(1)** was polymerized with sebacic acid **(2)** in different stoichiometries, yielding PXS pre-polymers **(3)**. A simplified representation of the pre-polymers is shown. **(B)** Pre-polymers of different stoichiometric ratios (PXS 1:1, PXS 2:3 and PXS 1:2) as well as a 50/50 w/w mixture of PXS 1:1/PXS 1:2 pre-polymers were further polymerized into elastomeric networks **(4)**. R can be hydrogen, xylitol or sebacic acid.

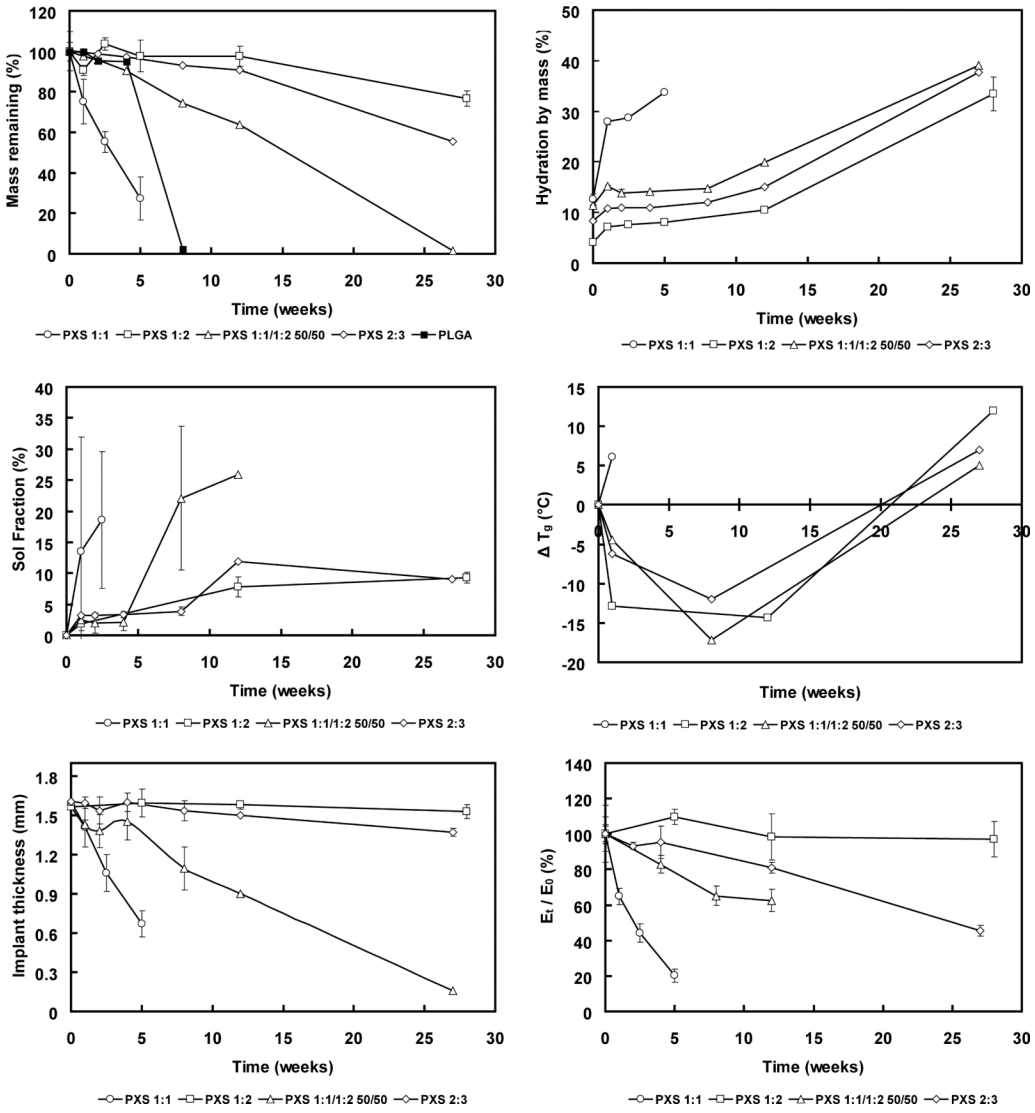

Figure 1.

In vivo behavior of PXS elastomers over time. Mass loss (including PLGA) **(A)**, implant thickness **(B)**, hydration by mass **(C)**, sol fraction **(D)**, mechanical properties **(E)** and ΔTg **(F)**. See Supplementary Figure 3 for PLGA hydration and mechanical properties over time.

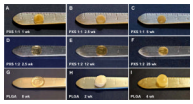

Figure 2.
Macroscopic morphology of implants: PXS 1:1 became opaque after 1 week **(A)** but did not swell during degradation, at 2.5 **(B)**, and 5 **(C)** weeks. PXS 1:2 implants remained optically transparent after 2.5 **(D)** and 12 **(E)** weeks, and became slightly opaque after 28 **(F)** weeks of implantation. PLGA implants **(G)** became swollen and opaque after 2 **(H)** and 4 **(I)** weeks of implantation.

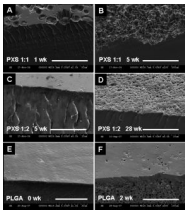

Figure 3.

SEM micrographs of PXS and PLGA implants. Representative images of PXS 1:1 at 1 week (bar represents 50 μm) **(A)**, and at 5 weeks in vivo (bar represents 500 μm) **(B)** are shown. PXS 1:2 at 5 weeks (bar represents 10 μm) **(C)**, and at 28 weeks in vivo (bar represents 10 μm) **(D)**, as well as PLGA at 0 weeks (bar represents 30 μm) **(E)** and 2 weeks in vivo (bar represents 100 μm) **(F)** are shown.

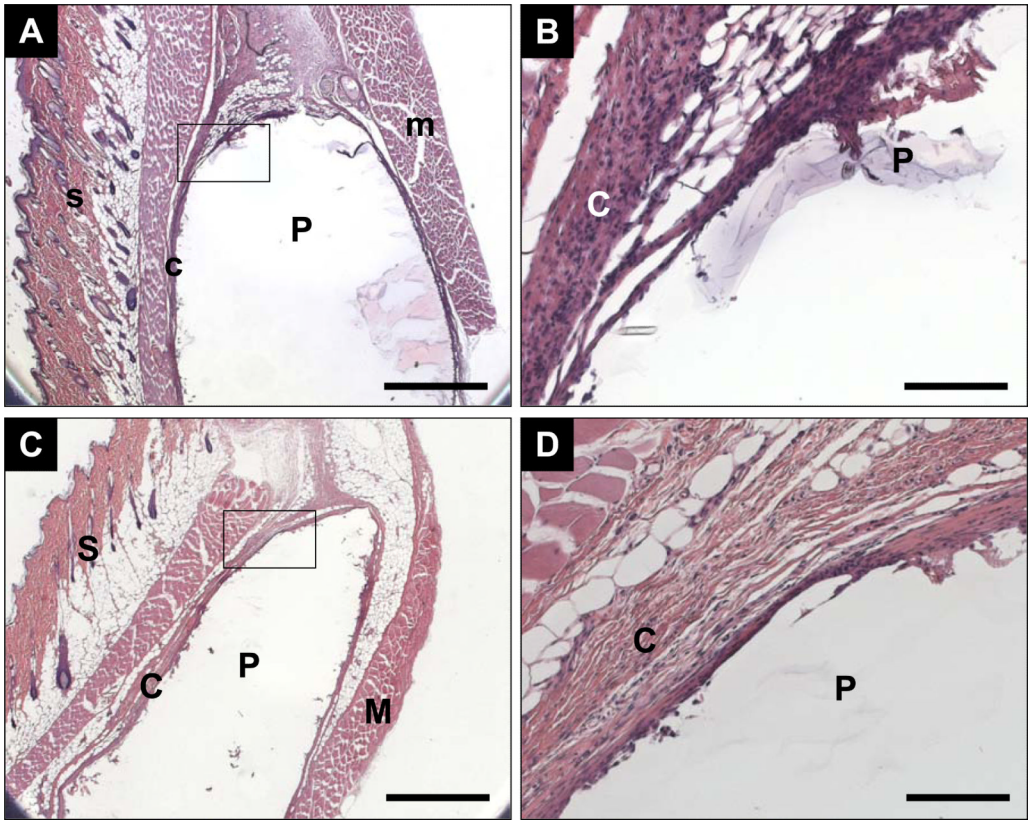

Figure 4.

Representative H&E stained sections of subcutaneously implanted PXS 1:1 discs. An overview of the acute inflammatory response surrounding PXS 1:1 implants at week 1 is shown at 2.5x **(A)** (bar represents 500 μm), and in more detail at 20x **(B)** (bar represents 75 μm). An overview of the chronic foreign body response surrounding degrading PXS 1:1 implants at 5 weeks is shown at 2.5x **(C)** (bar represents 500 μm), and in more detail at 20x **(D)** (bar represents 75 μm). The areas of the detailed images are represented in A and C by the black rectangular. P = polymer, C = fibrous capsule, S = skin and M = muscle.

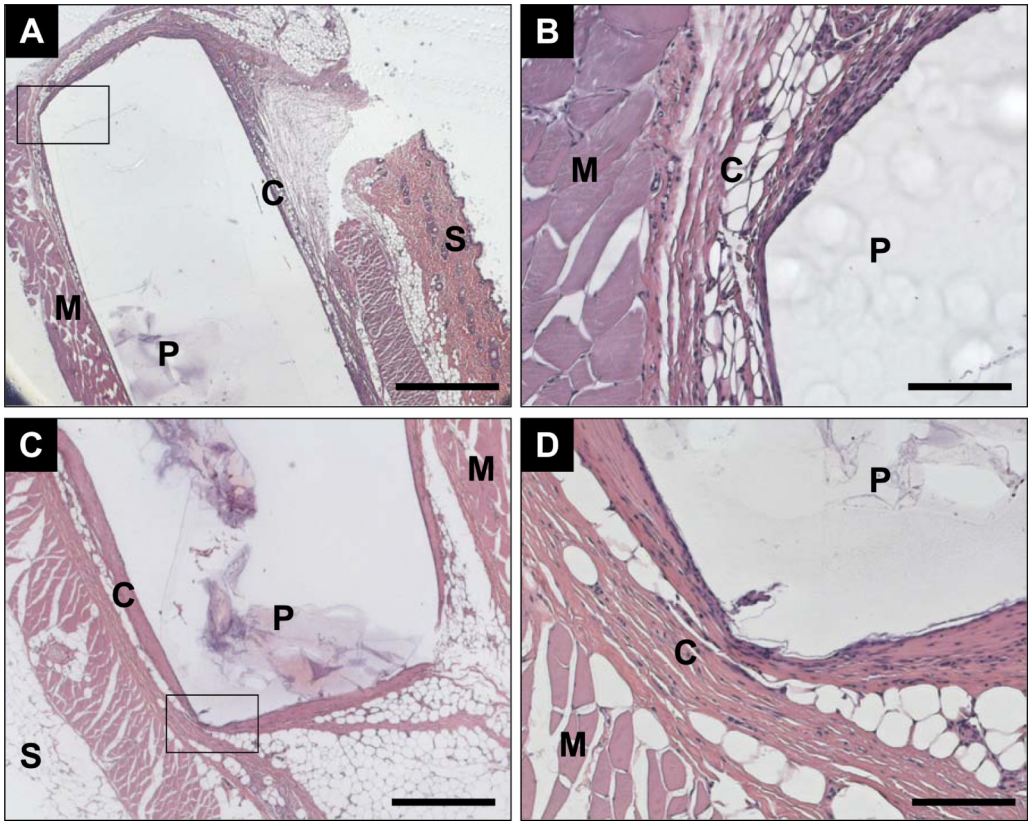

Figure 5.

Representative H&E stained sections of subcutaneously implanted PXS 1:2 discs. An overview of the acute inflammatory response surrounding PXS 1:2 implants at week 1 is shown at 2.5x **(A)** (bar represents 500 μm), and in more detail at 10x **(B)** (bar represents 150 μm). An overview of the chronic foreign body response surrounding degrading PXS 1:2 implants at 28 weeks is shown at 5x **(C)** (bar represents 250 μm), and in more detail at 20x **(D)** (bar represents 75 μm). The areas of the detailed images are represented in A and C by the black rectangular. P = polymer, C = fibrous capsule, S = skin and M = muscle.

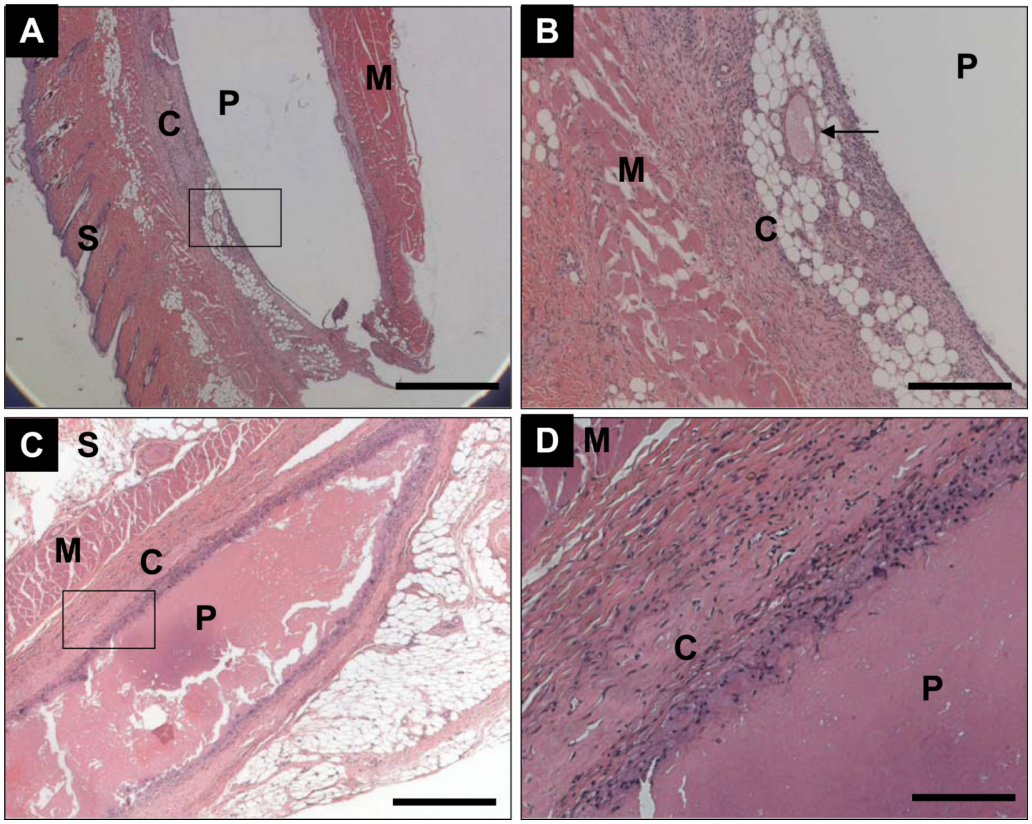

Figure 6.

Representative H&E stained sections of subcutaneously implanted PLGA discs. An overview of the acute inflammatory response surrounding PLGA implants at week 1 is shown at 2.5x **(A)** (bar represents 500 μm), and in more detail at 10x **(B)** (bar represents 150 μm). An overview of the chronic foreign body response surrounding degrading PLGA implants at 12 weeks is shown at 5x **(C)** (bar represents 250 μm), and in more detail at 20x **(D)** (bar represents 75 μm). The areas of the detailed images are represented in A and C by the black rectangular. P = polymer, C = fibrous capsule, S = skin and M = muscle. The arrow points to a large vessel of the fibrous capsule surrounding the PLGA implant.

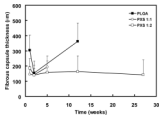

Figure 7.

Quantitative analysis of the in vivo foreign body response as measured by fibrous capsule thicknesses for PXS 1:1, 1:2 and PLGA implants. * indicates $p < 0.01$ between PXS 1:1 or PXS 1:2 and PLGA, as well as $p < 0.05$ between PXS 1:1 and PXS 1:2 at week 1. At week 12, ** indicates $p < 0.05$ between PXS 1:2 and PLGA (by non-parametric two-way ANOVA).

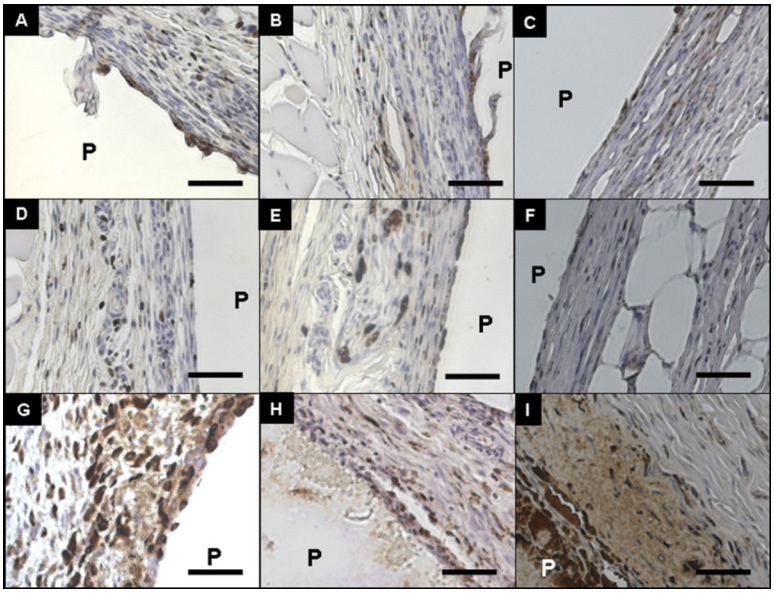

Figure 8.

Representative images of sections stained for CD68 (a marker of recruited and activated macrophages)13 of subcutaneously implanted PXS and PLGA discs. All images are magnified at 20x (bars represent 25 μm). Fibrous capsules surrounding PXS 1:1 at 1 **(A)**, 2 **(B)** and 5 weeks **(C)** showed CD68+ cells, similar to the PXS 1:2 at 1 **(D)**, 2 **(E)** and 12 weeks **(F)**. Fibrous capsules surrounding the PLGA implants seemed to have more CD68+ cells at 1 **(G)**, 2 **(H)** and 12 weeks **(I)**.

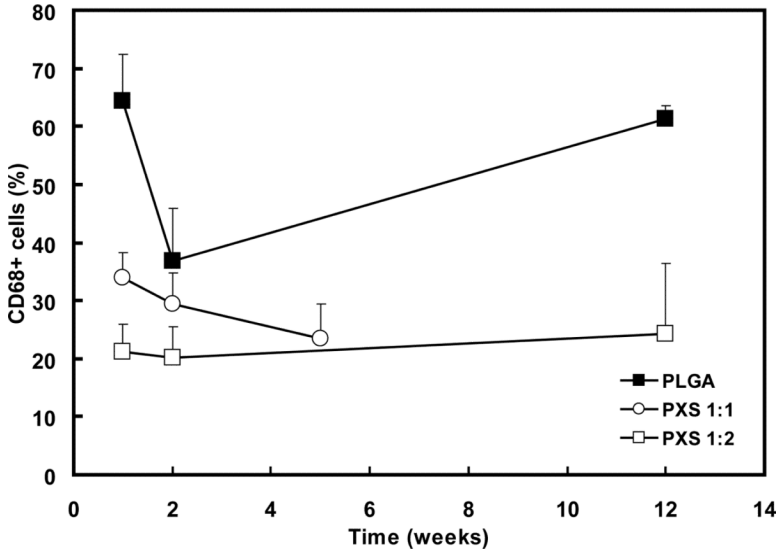

Figure 9.

Quantitative analysis of in vivo biocompatibility expressed by the fraction of activated macrophages (CD68+) within the fibrous capsules surrounding the implants. Significance levels were determined by non-parametric two-way ANOVA (* $p < 0.05$ for PXS 1:1 and PLGA at week 1, ** $p < 0.001$ for PXS 1:2 and PLGA at week 1, § $p < 0.05$ for PXS 1:2 and PLGA at week 2, and *** $p < 0.001$ for PXS 1:2 compared to PLGA at week 12).

Table 1

Properties of PXS pre-polymers.

Pre-polymer	Composition by ^{1}H-NMR	T_m [a] (°C)	M_w (g/mol)	M_n (g/mol)	*PDI*
PXS 1:1	1.0 : 0.91	80	2443	1268	1.9
PXS 1:1/1:2	1.0 : 1.56	90	4690	1689	2.8
PXS 2:3	1.0 : 1.63	100	3156	1117	2.7
PXS 1:2	1.0 : 1.85	100	6202	2255	2.7

[a] T_ms are temperatures where the polymer revealed a transition from a white, opaque wax to an optically transparent liquid.

Table 2

Physical and mechanical properties of PXS elastomers. M_C: the molecular weight between crosslinks, and n: crosslink density, both calculated from Eqn. 1 (Materials and Methods).

Polymer	Curing process	Young's Modulus (MPa)	Compression Modulus (MPa)	T_g (°C)	Contact angle (°)	Hydration by mass (%)	ρ (g/cm^3)	n (mol/m^3)	M_c (g/mol)
PXS 1:1	120 °C, 2 Pa, 4 d	0.82 ± 0.15	1.67 ± 0.20	7.3	26.5 ± 3.6	12.6 ± 0.4	1.18 ± 0.02	112.2 ± 30.5	10517.4 ± 102.1
PXS 1:1/1:2	120 °C, 2 Pa, 4 d	2.32 ± 0.27	2.67 ± 0.59	18.7	31.6 ± 4.3	8.3 ± 1.6	1.17 ± 0.03	317.4 ± 21.0	3685.7 ± 90.5
PXS 2:3	120 °C, 2 Pa, 4 d	3.42 ± 0.13	3.71 ± 0.20	20.2	43.8 ± 2.2	3.7 ± 0.9	1.18 ± 0.01	468.0 ± 29.2	2521.6 ± 100.5
PXS 1:2	120 °C, 2 Pa, 4 d	5.33 ± 0.40	5.68 ± 0.56	22.9	52.7 ± 5.7	4.1 ± 0.3	1.16 ± 0.02	729.3 ± 57.3	1585.1 ± 43.7